JOURNAL OF CATALYSIS 132, 58–67 (1991)

Magnesia-Supported Nickel Catalysts

I. Factors Affecting the Structure and Morphological Properties

F. ARENA,* B. A. HORRELL,†,[1] D. L. COCKE,† A. PARMALIANA,‡,[2] AND N. GIORDANO*

*Istituto CNR-TAE, Salita S. Lucia 39, 98126 S. Lucia, Messina, Italy; †Department of Chemistry, Texas A&M University, College Station, Texas 77843; and ‡Dipartimento di Chimica Industriale, Universitá di Messina, Salita Sperone, C.P. 29, 98166 S. Agata, Messina, Italy

Received June 29, 1990; revised January 3, 1991

The effects of calcination and reduction temperature on the metal dispersion of MgO-supported Ni in the ranges 400–800°C and 300–800°C, respectively, have been systematically evaluated by hydrogen chemisorption measurements and comparison has been made with a NiO–MgO physical mixture. The role of the bulk $Ni_xMg_{(1-x)}O$ solid solution in controlling NiO reducibility and the metal dispersion of Ni/MgO has been ascertained by XPS and ISS investigations. A mechanistic model accounting for the nickel oxide dispersion across the MgO support and the consequent formation of the bulk $Ni_xMg_{(1-x)}O$ solid solution has been proposed. A linear relationship between the mean particle size and the reduction temperature, the slope of which increases with Ni loading (2.8–18.0 wt%), has been found. A "multilayer arrangement" of Ni precursor on the support is discussed.

INTRODUCTION

The great interest focused on supported nickel systems in recent years has allowed rational understanding of their catalytic behavior. From numerous investigations devoted to the physicochemical characterization of Ni-supported catalysts (*1–6*), general agreement has been reached on two fundamental issues: (i) the factors affecting the morphological properties and (ii) the role of surface features on the reactivity. Bartholomew and Sorensen (*1*), studying the sintering of Ni/Al_2O_3 and Ni/SiO_2 catalysts, stated that: (a) the loss of metal surface area (MSA) occurs as a result of metal crystallite growth and support collapse; (b) the mechanism of sintering shifts from "crystallite migration" to "atomic migration" with increasing temperature and time of sintering. Tamagawa *et al.* (*2*) claimed that the Ni particle size in silica-supported Ni catalysts, prepared by the alkoxide technique, can be controlled by prescribing the calcination and reduction temperature, as well as by the extent of metal loading. Strong metal support interaction (SMSI) has been invoked in order to explain the competitive adsorption pattern of CO and H_2 on Al_2O_3 and TiO_2-supported nickel (*3, 4*). In addition, the influences of metal loading and preparation method on the catalytic properties of several Ni-based systems have been ascertained (*5, 6*).

Nevertheless, in spite of extensive knowledge achieved on conventional supported nickel catalysts, systematic and basic evaluations dealing with the factors controlling the bulk and the surface structure of Ni/MgO systems are still lacking. The reducibility of NiO/MgO is controlled by the extent of NiO–MgO solid solution (*7–10*) and therefore its reactivity is markedly dependent on the calcination temperature (*11, 12*). In this respect, Parmaliana *et al.* (*11*), who found a direct correlation between the catalytic activity in methane steam reforming and the NiO reducibility, reported that calcination temperatures higher than 400°C render the final Ni/MgO catalysts progressively less active. Meanwhile Narayanan

[1] Present address: Texaco Research, Austin, TX.
[2] To whom correspondence should be addressed.

0021-9517/91 $3.00

and Sreekanth (*13*), studying the availability of Ni on different carriers, found Ni/MgO to be the least reducible and the most dispersed system. However, no typical SMSI effects can be invoked to describe this peculiar behavior (*14*).

The present investigation aims to shed light on the influence of thermal treatments (i.e., calcination and reduction) and of the extent of Ni loading on the metal surface structure of Ni/MgO catalysts, and to propose a mechanism for the effects.

EXPERIMENTAL

Catalysts

Supported nickel on magnesia catalysts (MPF) were prepared by the incipient wetness method, according to the procedure described elsewhere (*10*), using MgO "smoke" powder (UBE Ind. Ltd., Japan, high purity grade product; BET surface area 34 $m^2 g^{-1}$; pore volume 0.230 $cm^3 g^{-1}$) as support. A NiO–MgO physical mixture (PM) was prepared by mixing predetermined amounts of MgO smoke powder and NiO powder (obtained by thermal decomposition of $Ni(NO_3)_2 \cdot 6H_2O$ at 400°C under an air stream).

In order to ascertain the effect of the calcination temperature (T_c) on the structural properties several aliquots of dried MPF 12 catalyst (18.0 wt% Ni) and the PM sample (13.3 wt% Ni) were calcined in air for 16 h at temperatures ranging between 400 and 800°C. Heat treatments and nickel loadings, as determined by atomic adsorption (AAS) measurements, are summarized in Table 1.

TABLE 1

List of Samples Studied

Preparation method	Sample	T_c[a] (°C)	Ni loading (wt%)	BET S.A. ($m^2 g^{-1}$)
Incipient wetness	MPF 12-std	400	18.0	37
	MPF 12-6	600	18.0	29
	MPF 12-7	700	18.0	—
	MPF 12-8	800	18.0	22
	MPF 13-std	400	2.8	36
	MPF 15-std	400	10.8	36
Mechanical mixing	PM-std	400	13.3	—
	PM-6	600	13.3	—
	PM-7	700	13.3	—
	PM-8	800	13.3	—

[a] All samples were calcined at the listed temperature (T_c) for 16 h.

Hydrogen Chemisorption Measurements

Hydrogen chemisorption data were obtained by flow thermal desorption tests (*15*), using a conventional flow apparatus operating both in continuous and pulse mode. Hydrogen (SiO Ind., Italy, purity >99.95%) and nitrogen carrier gas (SiO Ind., Italy, purity >99.95%) were further purified by activated molecular sieves and Oxy Absorbent (Alltech product) traps, kept at room temperature (RT) to remove respectively any water and oxygen.

Catalysts and physical mixture samples (0.2–0.4 g; 40–70 mesh fraction) were placed in a tubular quartz U-microreactor and reduced for half an hour in a hydrogen flow (1.5 STP liter h^{-1}) at a temperature (T_r) ranging from 300 to 800°C. After the reduction treatment, the sample was cooled in flowing H_2 to room temperature, equilibrated for 30 min, and then further cooled in a dry ice–ethanol bath to −72°C, equilibrating for 15 min. Then the H_2 was shut off and the sample was purged with the nitrogen carrier flow (1.8 STP liter h^{-1}) for 20 min. After purging, the dry ice–ethanol bath was removed and the U-reactor was quickly placed into a furnace preheated at 530°C (this temperature was selected in order to obtain a symmetric desorption peak). The desorption process, lasting about 5 min, was monitored and quantified by a thermal conductivity detector (TCD) connected to a HP 3396 A integrator. After every desorption run a calibration test was performed by injecting in the carrier gas a

known amount of H_2 in order to obtain reliable quantitative measurements. Metal dispersion (**D**) was calculated from the following experimental ratio by assuming the chemisorption stoichiometry $H/Ni_{surf} = 1$:

$$\mathbf{D}(\%) = (X_{H_2}/X_{O_2}) \cdot 100,$$

where X_{H_2} is the hydrogen uptake (μmol g_{cat}^{-1}) and X_{O_2} is the oxygen uptake (μmol g_{cat}^{-1}) at 450°C, which corresponds to the fraction (α) of NiO reduced to Ni^0 according to the following oxidation stoichiometry: $Ni^0 + \frac{1}{2}O_2 = NiO$ (*3*). Metal surface area (MSA, $m_{Ni}^2\, g_{cat}^{-1}$) was calculated assuming a Ni site density of 6.5 Å^2/atom (*4*), while the Ni mean particle size ($\mathbf{d}_s$) was derived from the equation:

$$\mathbf{d}_s(\text{Å}) = 971/\mathbf{D}(\%)$$

as suggested by Bartholomew *et al.* (*3*).

X-Ray Photoelectron Spectroscopy Measurements

XPS measurements were performed with a Kratos XSAM800 spectrometer (180° hemispherical analyzer) dual anode X-ray source fitted to a specially designed spherical vacuum chamber. The Mg anode (1256.3 eV) used was run at 12 kV and 10 mA. A Kratos DS 800 operating system was used to control data acquisition and software was utilized for the raw peak area determination. XPS areas were calculated using the total integrated area of Mg 2*p*, Ni $2p_{3/2}$, O 1*s*, and C 1*s* regions. Areas were normalized using sensitivity factors (*16*) and the total number of scans. Peak positions were calibrated using the C 1*s* ("adventitious carbon") photoelectron peak at 285.0 eV (B.E.) as reference.

Ion-Scattering Spectroscopy Analysis

A Kratos ion scattering spectrometer with a 137° solid acceptance angle cylindrical mirror analyzer (CMA), equipped with a coaxially mounted mini beam ion gun, capable of producing beam diameters from about 100 μm to several millimeters and currents from tens of nanoamps to one to two microamps at beam energies up to 4000 eV, was used to obtain the ISS data. All ISS results were obtained using a rastered 1-mm-diameter 2000-eV $^4He^+$ beam which was focused onto the sample located about 6 mm from the plane of the CMA entrance. All the samples required charge neutralization. A typical scan from 2000 eV took approximately 4 s to complete. Scans were collected in a logarithmic fashion in order to provide a depth profile of each detected species.

RESULTS

Hydrogen Chemisorption

Hydrogen uptakes and NiO reducibility values (α,%) of differently loaded Ni/MgO catalysts (2.8–18.0 wt% Ni), air calcined in the T_c range 400–800°C, are listed in Table 2. NiO reducibility increases with Ni load-

TABLE 2

Hydrogen Chemisorption on Ni/MgO Catalysts

Catalyst	T_r[a] (°C)	α (%)	H_2 uptake (μmol g_{cat}^{-1})	**D** (%)	$\mathbf{d}_s$ (Å)
MPF 12-std	300	13.6	46.4	22.7	43
MPF 12-std	400	26.0	92.1	23.1	42
MPF 12-std	600	47.3	106.7	14.7	66
MPF 12-std	725	68.0	111.9	10.8	90
MPF 12-std	800	76.5	107.6	9.1	107
MPF 12-6	500	25.0	42.4	11.1	87
MPF 12-6	600	32.0	54.7	11.2	87
MPF 12-6	725	47.3	69.1	9.6	101
MPF 12-6	800	62.0	72.7	7.6	128
MPF 12-7	600	15.6	40.4	16.9	57
MPF 12-7	725	25.0	51.1	13.3	73
MPF 12-8	500	0.8	11.2	90.0	11
MPF 12-8	600	2.6	15.8	36.8	26
MPF 12-8	725	6.3	26.4	27.3	36
MPF 12-8	800	11.2	38.9	22.6	43
MPF 13-std	400	10.5	19.7	78.7	12
MPF 13-std	600	27.8	34.6	52.0	19
MPF 13-std	800	54.7	36.8	28.2	34
MPF 15-std	400	9.0	62.0	67.0	15
MPF 15-std	600	36.0	89.7	27.5	35
MPF 15-std	800	61.0	117.9	18.5	53

Note. α, NiO reducibility (Ni^0/Ni_{tot}). **D**, Metal dispersion (Ni_{surf}^0/Ni^0). $\mathbf{d}_s$, Average crystallite size.

[a] All samples were reduced at the listed T_r for 30 min.

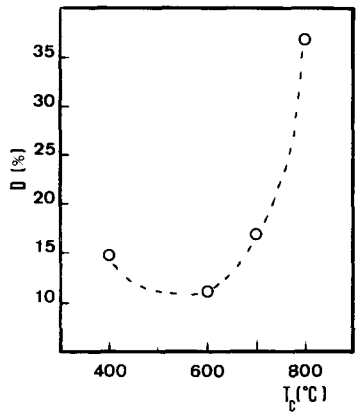

FIG. 1. Effect of the calcination temperature (T_C) on metal dispersion, **D**(%), of the MPF 12 catalyst (18.0 wt% Ni). T_r = 600°C.

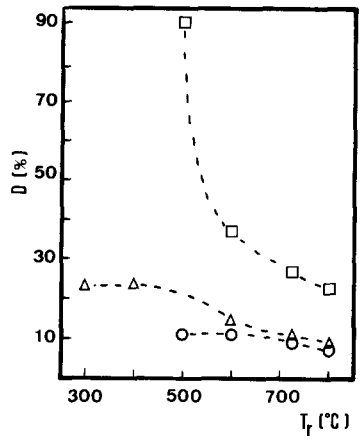

FIG. 2. Effect of the reduction temperature (T_r) on metal dispersion, **D**(%), of the MPF 12 catalysts: △, MPF 12-std (T_C = 400°C); ○, MPF 12-6 (T_C = 600°C); □, MPF 12-8 (T_C = 800°C).

ing and reduction temperature (T_r), while high calcination temperatures (T_c > 400°C) cause a markedly decreased reducibility. The MgO support did not show any hydrogen adsorption or oxygen consumption under the above experimental conditions.

The trend of metal dispersion (**D**) with calcination temperature observed for MPF 12 catalyst (18.0 wt% Ni) reduced at 600°C is depicted in Fig. 1. **D** is not significantly affected by T_c up to 700°C, but it substantially increases at 800°C.

A comprehensive view of the effects of T_r on the metal dispersion of different air-calcined MPF 12 samples is shown in Fig. 2. The metal dispersion of the MPF 12-std and MPF 12–6 samples does not change for T_r lower or equal to T_c, while it decreases gradually at T_r higher than T_c. Moreover, a dramatic drop of **D**, in the whole experimental range of T_r (500–800°C), is observed for the MPF 12–8 sample.

The structural properties of the MPF 12 catalysts are summarized in Fig. 3 showing the relationship between the MSA ($m^2_{Ni}\ g^{-1}_{cat}$) and the NiO reducibility (α,%). The MSA of the MPF 12-std and MPF 12-6 samples increases with the degree of reduction to reach a maximum, whereas for the MPF 12-8 sample a linear increase of MSA with α has been found.

Figure 4 shows the effect of T_r on the mean crystallite size ($\mathbf{d}_s$) of differently loaded Ni/MgO catalysts calcined at 400°C. For all the samples $\mathbf{d}_s$ increases regularly with T_r. Moreover the rate of growth of $\mathbf{d}_s$ with T_r ($\Delta\ \mathbf{d}_s/\Delta T_r$, Å/°C) increases with increasing the metal content.

Finally, in Table 3 are collected the values of NiO reducibility, hydrogen uptake,

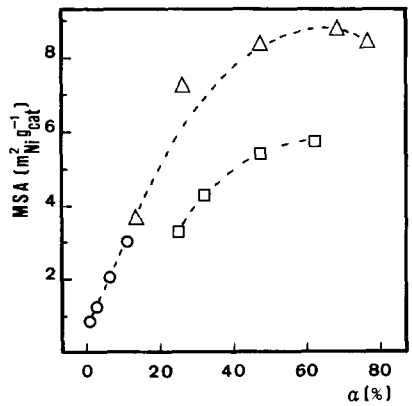

FIG. 3. Influence of the NiO reduction degree, α(%), on the metal surface area (MSA) of different air-calcined MPF 12 catalysts: △, MPF 12-std (T_C = 400°C); □, MPF 12-6 (T_C = 600°C); ○, MPF 12-8 (T_C = 800°C).

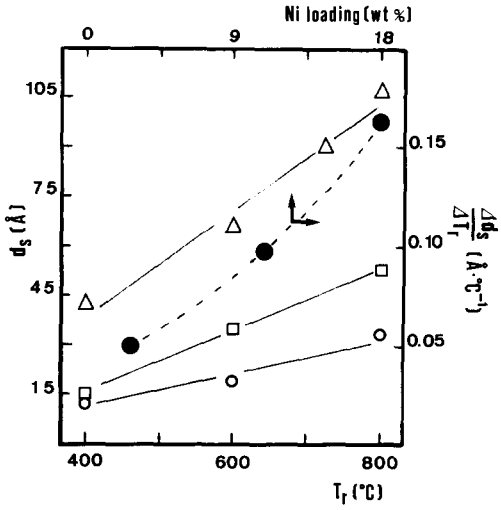

FIG. 4. Effect of the reduction temperature (T_r) on the mean Ni crystallite size ($\mathbf{d}_s$) of Ni/MgO catalysts with different metal loading: ○, MPF 13-std (2.8 wt% Ni); □, MPF 15-std (10.8 wt% Ni); △, MPF 12-std (18.0 wt% Ni). ●, Relationship between the Ni loading and the growth rate of $\mathbf{d}_s$ with T_r ($\Delta\mathbf{d}_s/\Delta T_r$).

and metal dispersion for the air-calcined PM samples (13.3 wt% Ni). In the mechanically mixed system NiO reducibility becomes considerably lower than 100% at $T_c \geq 700$°C only. However, the unusual trend of metal dispersion with Tc, on the whole, looks similar to that found on the Ni/MgO supported system.

XPS

Ni 2*p* (A) and O 1*s* (B) regions of XPS spectra of MPF 12 samples, air-calcined in the T_c range 400–800°C, are shown in Fig. 5. These spectra indicate immediately that calcining at high T results in a decreased Ni^{2+} surface concentration. At the same time, the total surface composition (Ni, Mg, O), outlined in Fig. 6(A), illustrates well the modifications occurring in the outermost structure of MPF 12 owing to the different calcination treatments, namely that a high T_c induces a progressive Ni depletion from the surface, enhancing in parallel the Mg concentration. This structural rearrangement is also confirmed by the changes observed in the shape of the O 1*s* peak (Fig. 5(B)). Indeed a high T_c leads to less "nickel oxide type" oxygen (B.E., 529.5 eV) to relative "magnesia type" (B.E., 531.4 eV).

In addition, the trend with T_c of the "normalized" XPS ratio **R** (**R** = R_T/R_{400}) pre-

TABLE 3

Hydrogen Chemisorption on PM Samples

Sample	T_r[a] (°C)	α (%)	H_2 uptake (μmol g_{PM}^{-1})	**D** (%)	$\mathbf{d}_s$ (Å)
PM-std	300	86.5	15.7	1.6	607
PM-std	400	98.0	15.6	1.4	694
PM-6	400	93.5	24.6	2.3	422
PM-7	400	69.0	28.1	3.7	262
PM-8	400	1.7	8.8	46.3	21

[a] All samples were reduced at the listed T_r for 30 min.

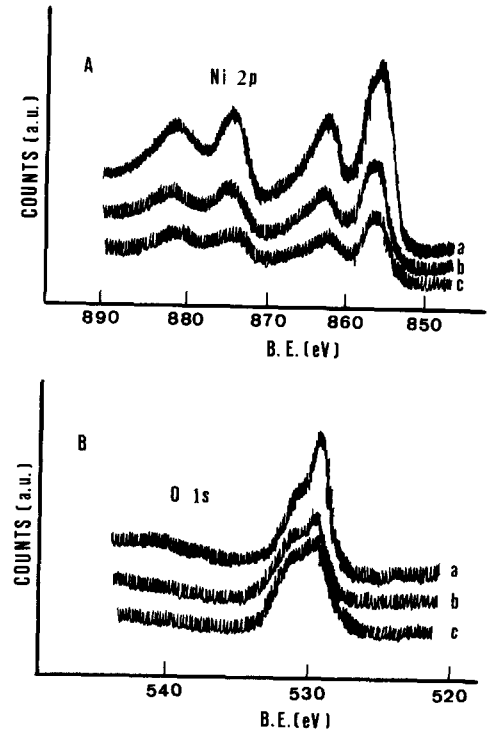

FIG. 5. XPS spectra of the air-calcined MPF 12 catalysts: (a) MPF 12-std (T_C = 400°C); (b) MPF 12-6 (T_C = 600°C); (c) MPF 12-8 (T_C = 800°C). (A) Ni 2*p* region; (B) O 1*s* region.

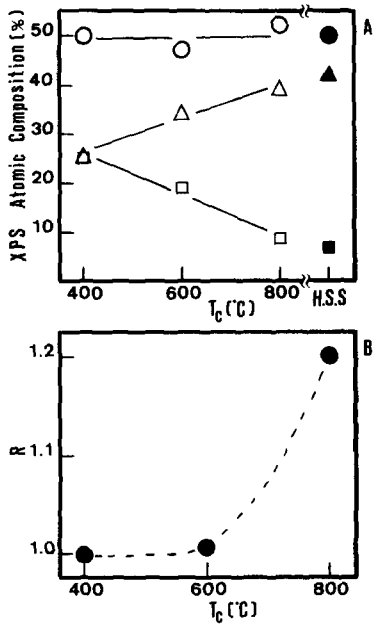

FIG. 6. (A) Effect of calcination temperature (T_C) on the XPS atomic composition (%) of the MPF 12 catalyst: □, Nickel; △, Magnesium; ○, Oxygen. For comparison also the atomic composition, ■▲●, of a homogeneous solid solution (HSS) is shown. (B) Effect of T_C on the "normalized" XPS ratio **R** (**R** = R_T/R_{400}, where respectively R_T and R_{400} are the ratios between C 1*s* from carbonate carbon and Mg 2*p* peaks at $T_C = T$ and T_C = 400°C).

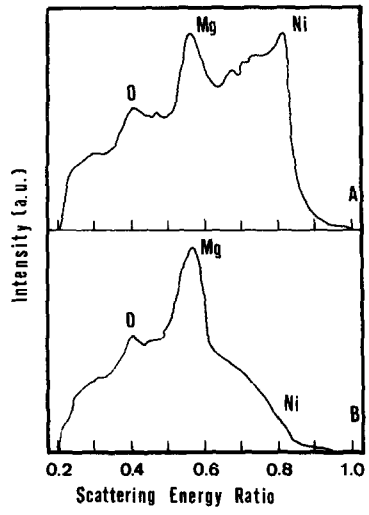

FIG. 7. ISS spectra of air-calcined MPF 12 catalysts: (A) MPF 12-std and (B) MPF 12-8. 1 min of sputtering.

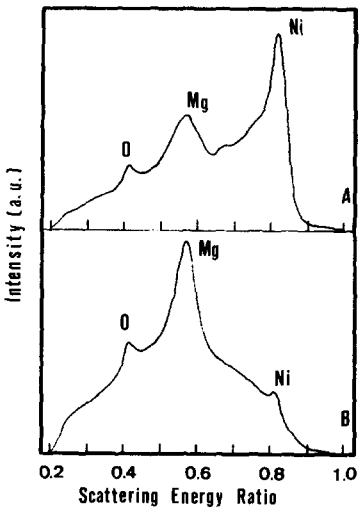

FIG. 8. ISS spectra of air-calcined MPF 12 catalysts: (A) MPF 12-std and (B) MPF 12-8. 20 min of sputtering.

sented in Fig. 6(B), where respectively R_T and R_{400} are the ratios at $T_c = T$ and T_c = 400°C between the C 1*s* peak from carbonate carbon (B.E., 287.9 eV) and the Mg 2*p* peak, indicates an enhanced "surface basicity" (preponderance of MgO-type surface) for the systems calcined at high T_c.

ISS

ISS profiles of the MPF 12-std and MPF 12-8 samples, after 1 min and after 20 min of sputtering, are shown in Figs. 7 and 8, respectively (the MPF 12-6 spectra are similar to those of MPF 12-std).

The 1-min spectra, giving a more accurate picture of the initial surface composition, appear quite different for each of two investigated systems. For the MPF 12-std sample there are scattering peaks due to oxygen, magnesium, and nickel, with the major portion being nickel. The pertinent spectrum of the MPF 12-8 sample (Fig. 8) presents significant differences: there is much more magnesium on the surface and very little, if any, nickel detected.

After 20 min of sputtering we note on the MPF 12-8 sample a considerable growth of

the Ni peak, with the Mg still predominant, while for the MPF 12-std sample the Ni peak becomes the largest in the spectrum.

DISCUSSION

Effect of Calcination Temperature (T_c)

In recent studies dealing with the NiO–MgO interaction, we pointed out that the calcination temperature induces substantial modifications in the reduction pattern of several Ni/MgO systems (*9, 10*). In particular, the diffusion of NiO into the MgO structure, with the consequent formation of NiO–MgO solid solutions, controls the whole reducibility (*10*). Previously, Highfield *et al.* (*7*), studying the catalytic properties of Ni/MgO and Co/MgO derived from NiO–MgO and CoO–MgO solid solutions, attributed their high metal dispersions to the structural peculiarities of the solid solutions. On this account, we can explain the trend of the "reduction isotherm" (T_r = 600°C) outlined in Fig. 1 by inferring that the calcination treatment affects the structure of the MPF 12 catalyst (18.0 wt% Ni/MgO), producing marked changes either in NiO reducibility or nickel dispersion. Namely, the hydrogen treatment at 600°C of the MPF 12-std sample (T_c = 400°C) allows the reduction of a considerable fraction of the NiO located on the surface and in the near surface regions of the MgO support (*10*), giving rise to surface Ni^0 dispersed moderately (**D** = 14.7%). By contrast, in the MPF 12-8 sample (T_c = 800°C) NiO is "dissolved" as small subsurface clusters (*7*) into the MgO lattice forming a quasi-homogeneous NiO–MgO solid solution (*10*). At T_r = 600°C the incipient reduction of these NiO particles yields a more dispersed system (**D** = 36.8%) owing to the low extent of NiO reducibility (2.6%) which hinders significant sintering. Furthermore, 600°C is not a T_c high enough to promote "wide" diffusion of NiO into the matrix (*10*). Then the less pronounced minimum of metal dispersion observed for the MPF 12-6 catalyst is likely to be attributable to a lower NiO dispersion, similar to that observed for Ni/Al_2O_3 catalysts (*17*). However, the improved **D** of the MPF 12-7 catalyst (T_c = 700°C), together with its lower reducibility, denote the incipient dissolution of NiO clusters into the MgO structure leading to an enhanced extent of unreducible $Ni_xMg_{(1-x)}O$ bulk solid solution with the consequent lowering of the Ni particle size in the reduced system (see Table 2).

XPS results help us to support further this view. Indeed, the progressive lowering both of the Ni 2*p* and oxygen 1*s* type NiO bands, for catalysts calcined at higher T_c (see Fig. 5), is confirmatory evidence of the surface Ni depletion, which negatively affects the reducibility of the Ni/MgO system (*8*). Moreover, from the quantitative evaluation of the surface chemical composition (Fig. 6 (A)) emerges the tendency of the system to rearrange its structure until reaching at 800°C a "quasi-steady-state" corresponding to an ideal and homogeneous solid solution, still showing a slight surface Ni segregation. The lower surface Ni concentration of the MPF 12-6 catalyst is related both to the above inferred NiO sintering and to the increased extent of NiO dissolved in the bulk of the support. The progressive surface carboxylation of samples treated at high T_c (see Fig. 6 (B)) could reflect a higher "surface basicity" linked with the NiO migration toward the MgO bulk. This hypothesis is further supported by the ISS analysis showing a large overlaying of Mg and the nearly complete disappearance of Ni from the MPF 12-8 surface (Fig. 7). Furthermore, the growth of the ISS Ni peak in the MPF 12-8 sample and the lowering of Mg in the MPF 12-std case, recorded after 20 min of sputtering (Fig. 8), are associated with the removal of a thin MgO layer probably appearing on the surface as a consequence of its more pronounced reactivity toward the atmosphere.

Therefore, our experimental data seem to be consistent with a reaction mechanism involving a mobility of Ni^{2+} ions across the MgO structure, adequate to give the forma-

tion of a bulk $Ni_xMg_{(1-x)}O$ solid solution. Indeed, we can infer that: (i) upon T_c increase from 400 to 600°C, surface "free" NiO clusters (*10*) agglomerate in larger particles lowering the "lattice distortion" and consequently their reduction rate (*18*); (ii) for T_c higher than 600°C Ni^{2+} ions quickly diffuse into the matrix and the system evolves progressively toward an "equilibrium state" corresponding to the bulk $Ni_xMg_{(1-x)}O$ solid solution. On the basis of the above considerations, the mechanism scheme presented in Fig. 9 depicts well the structural modifications occurring in Ni/MgO catalysts as T_c increases from 400 to 800°C. In particular, it accounts for the marked tendency of NiO and MgO to interact according to a mechanism of lattice substitution that at high T_c leads to a system almost homogeneously "mixed" (MPF 12-8).

For the PM series, both H_2 chemisorption and NiO reducibility data provide evidence for a trend similar to that observed on the Ni/MgO-supported catalysts (see Table 3). Indeed, the reduction at 400°C leads to a very low metal dispersion (**D** = 1.5%) in the PM-std sample (T_c = 400°C), which suddenly increases in the PM-8 sample (T_c = 800°C) to a value (**D** = 46.3%) comparable with those of the corresponding MPF 12-8 catalyst. The higher NiO reducibility and the lower Ni dispersion of the PM samples, compared to the MPF 12 catalysts, are attributable to the preparation methods enabling a different "contact area" between NiO and MgO (*10*).

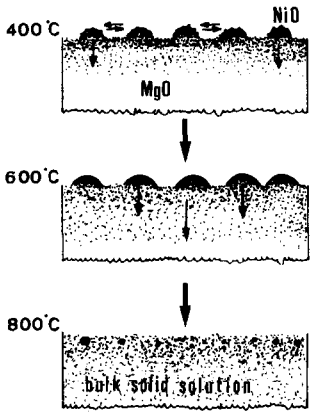

FIG. 9. Mechanism scheme of NiO–MgO interaction at different T_C.

On the whole our results indicate an *entropic* reactivity governing the NiO–MgO interaction. The influence of the preparation method, strongly affecting the structure and the morphological properties of NiO/MgO systems for Tc ≤ 600°C, becomes of less importance at 800°C.

Effect of Reduction Temperature (T_r)

The observed negative influence of higher T_r on metal dispersion of the MPF 12 system (Fig. 2) reflects the typical behavior of supported metal catalysts. Nevertheless, we can consider that high T_r affects peculiarly the metal surface properties of the Ni/MgO system by the concurrence both of a physical and a chemical phenomenon, respectively: (i) the sintering caused by the enhanced surface mobility of Ni particles; and (ii) the increased NiO reducibility giving rise to a larger amount of surface metal particles.

Taking into account these remarks and assuming that one oxide crystallite produces one nickel crystallite (*18*) the different trends of **D** with T_r, shown in Fig. 2, are to be ascribed to the different NiO morphology which is controlled by T_c. Indeed, the analogous value of **D** estimated for the MPF 12-std catalyst, reduced in the range 300–400°C (Fig. 2), can be related with the reduction of "free" NiO particles (*10*), having the same mean size, and leads to the ruling out of the occurrence of any sintering effects. Likewise, the chemisorption data for the PM-std samples, reduced in the same T_r range, give evidence for only a slight difference in NiO reducibility without any change in metal dispersion (see Table 3). For the MPF 12-6 sample the incipient reduction at 600°C of the small NiO clusters, displaced in the subsurface sites of the MgO support (*10*), could mask the incipient

sintering leading fortuitously to the same metal dispersion observed at T_r = 500°C. For both MPF 12-std and MPF 12-6 catalysts high T_r cause a gradual lowering of **D** explicable by the above phenomena (i) and (ii).

The very high metal dispersion (90%) of the MPF 12-8 sample reduced at 500°C confirms that the NiO forming the bulk $Ni_xMg_{(1-x)}O$ solid solution is dissolved into the MgO lattice as Ni^{2+} ions and their reduction leads to Ni clusters "quasi-atomically" dispersed. On increasing T_r the larger amount of surface Ni atoms, having a high mobility (*19*), undergoes dramatic sintering.

In any case the plot of the development of metal surface area (MSA, $m^2_{Ni}\ g^{-1}_{cat}$) against the NiO reducibility (see Fig. 3) clearly shows the role of the heat treatments (T_c and T_r) in determining the practical suitability of Ni/MgO catalysts. Thus, (a) at low degrees of reduced NiO ($\alpha < 60\%$) the reduction temperature exerts a positive effect on MSA, although a decreasing metal dispersion has been observed, while (b) for higher degrees of reduction ($\alpha > 60\%$) sintering predominantly affects the MSA. Therefore, the prevalence of each one of the effects (i) and (ii) could produce a relationship between α and MSA with a maximum, the value of which also depends on T_c. However, a T_c higher than 400°C must be avoided for attaining the largest metal surface area.

Effect of Metal Loading

Hydrogen and oxygen uptakes indicate that higher nickel loadings exert a promoting role on NiO reducibility and a negative effect on metal dispersion (see Table 2). Indeed, the hydrogen treatment at 400°C, involving the reduction of free NiO particles, allows for MPF 13-std (2.8 wt% Ni) and MPF 15-std (10.8 wt% Ni) samples a slight reducibility (ca. 10%) together with a high metal dispersion (respectively 78.7 and 67%), while a larger reducibility (ca. 25%) and a moderate **D** (ca. 23%) were observed for MPF 12-std catalyst (18.0 wt% Ni). These results could be explained by inferring a different distribution of the Ni precursor on the support. In particular, for Ni loadings up to 10.8 wt%, NiO is homogeneously "spread" on the support occupying its most reactive sites. This "monolayer" arrangement hinders the formation of large free NiO particles (*10*), limiting the reducibility of the system. In contrast, on the MPF 12-std catalyst a NiO multilayer is formed. This structure enhances the NiO reducibility leading to a moderate metal dispersion. Similarly, SMSI effects render low-loaded Ni/Al_2O_3 systems less reducible, favoring the formation of small Ni crystallites (*5*, *6*).

However, the linear relationship between the mean Ni particle size ($\mathbf{d}_s$) and T_r, found for catalysts with different metal loading (Fig. 4), denotes a general behavior pattern accounting for the surface properties of the Ni/MgO system. Moreover, since the slope of this correlation ($\Delta\mathbf{d}_s/\Delta T_r$) is an increasing function of the Ni content (Fig. 4), we conclude that the metal loading affects the morphological properties of Ni/MgO-supported system by controlling the distribution and the consequent reducibility of NiO onto the MgO support.

CONCLUSIONS

The surface properties of the NiO/MgO system are strongly connected with its propensity to form solid solutions. XPS and ISS evidence confirms that calcination at T_c higher than 600°C induces dramatic changes in the structure and the surface properties of Ni/MgO catalysts. Metal loading controls the NiO reducibility and the sintering of Ni particles without altering the general pattern. The optimum calcination temperature for gaining the highest metal surface area in magnesia-supported Ni catalysts is 400°C.

ACKNOWLEDGMENTS

The authors are very grateful to Dr. Francesco Frusteri (CNR-TAE, Messina) for helpful discussion and suggestions. The Ministero della Pubblica Istruzione

and CNR (Rome) are acknowledged for partial financial support.

REFERENCES

1. Bartholomew, C. H., and Sorensen, W. L., *J. Catal.* **81,** 131 (1983).
2. Tamagawa, H., Oyama, K., and Yamaguchi, T., *J. Chem. Soc. Faraday Trans 1* **83**(10), 3189 (1987).
3. Bartholomew, C. H., Pannell, R. B., and Butler, J. L., *J. Catal.* **65,** 335 (1980).
4. Smith, J. S., Thrower, P. A., and Vannice, M. A., *J. Catal.* **68,** 270 (1981).
5. Bartholomew, C. H., and Pannell, R. B., *J. Catal.* **65,** 390 (1980).
6. Narayanan, S., and Uma, K., *J. Chem. Soc. Faraday Trans 1* **81,** 2733 (1985).
7. Highfield, J. G., Bossi, A., and Stone, F. S., *in* "Preparation of Catalysts III" (G. Poncelet, P. Grange, and P. A. Jacobs, Eds.), p. 181. Elsevier, Amsterdam, 1983.
8. Bond, G. C., and Sarsam, S. P., *Appl. Catal.* **38,** 365 (1988).
9. Arena, F., Parmaliana, A., Frusteri, F., and Giordano, N., *React. Kinet. Catal. Lett.* **42,** 121 (1990).
10. Parmaliana, A., Arena, F., Frusteri, F., and Giordano, N., *J. Chem. Soc. Faraday Trans.* **86**(14), 2663 (1990).
11. Parmaliana, A., Frusteri, F., Arena, F., Mondello, N., and Giordano, N., *in* "Structure and Reactivity of Surfaces" (C. Morterra, A. Zecchina, and G. Costa, Eds.), p. 739. Elsevier, Amsterdam, 1989.
12. Takezawa, N., Terenuma, H., Shimokawabe, M., and Kobayashi, H., *Appl. Catal.* **23,** 291 (1986).
13. Narayanan, S., and Sreekanth, G., *J. Chem. Soc. Faraday Trans 1* **85**(11), 3785 (1989).
14. Maubert, A., Martin, G. A., Praliaud, H., and Turlier, P., *React. Kinet. Catal. Lett.* **22.** 203 (1983).
15. Jones, R. D., and Bartholomew, C. H., *Appl. Catal.* **39,** 77 (1988).
16. Briggs, D., and Seah, M. P., "Practical Surface Analysis by X-Ray Photoelectron and Auger Spectroscopy." Wiley, New York, 1983.
17. Chen, I., Lin, S. Y., and Shiue, D. W., *Ind. Eng. Chem. Res.* **27,** 926 (1988).
18. Coenen, J. W. E., *in* "Preparation of Catalysts II" (B. Delmon, P. Grange, P. A. Jacobs, and G. Poncelet, Eds.), p. 89, Elsevier, Amsterdam, 1979.
19. Richardson, J. T., and Crump, J. G., *J. Catal.* **57,** 417 (1979).